Chemistry–A European Journal
Research Article
doi.org/10.1002/chem.202202234
Chemistry Europe
European Chemical Societies Publishing
www.chemeurj.org

Special Collection

Charge-Transfer Transitions Govern the Reactivity and Photophysics of Vicinally Diphosphanyl-Substituted Diborapentacenes

Tao Jin,[a] Michael Bolte,[a] Hans-Wolfram Lerner,[a] Jan-Michael Mewes,*[b] and Matthias Wagner*[a]

Abstract: 2,3-Difluoro-5,14-dihydro-5,14-diborapentacene (DBP) was endowed with two vicinal Ph_2P groups by an S_NAr reaction at both CF sites using Ph_2PSiMe_3. Computations reveal the ambipolar product **P** to undergo P-to-B charge transfer under ambient light irradiation. Consequently, **P** is prone to photooxidation by air, yielding the $Ph_2P(O)$ species **PO**. With S_8 or $[Me_3O][BF_4]$, **P** furnishes the $Ph_2P(S)$ or $Ph_2P(Me)^+$ derivatives **PS** or [**PMe**][BF_4]$_2$. Along the series **P**, **PO**, **PS**, and [**PMe**][BF_4]$_2$, the redox potentials shift anodically from $E_{1/2} = -1.89$ V to -1.02 V (CH_2Cl_2). Thus, derivatization of the Ph_2P group allows late-stage modulation of the LUMO-energy level of the DBP. Derivatization also influences the emission properties of the compounds, as **PO** shows green (521 nm) and [**PMe**][BF_4]$_2$ red (622 nm) fluorescence in C_6H_6, while **P** and **PS** are dark. With CuBr and AgBr, **P** forms dimeric [M(μ-Br)]$_2$ complexes [**PCu**]$_2$ and [**PAg**]$_2$, which show pronounced metal-to-ligand charge transfer (MLCT), making **P** a promising ligand for photocatalysts.

Introduction

Numerous heterocyclic arylboranes stand out for their pronounced photoluminescence and electron-accepting qualities, which make them promising candidates for the development of novel optoelectronic materials.[1] As a rule of thumb, a more extended π-electron system and an increasing number of electron-deficient B atoms incorporated into it decrease the energy level of the lowest unoccupied molecular orbital (LUMO) of the compound, thus red-shifting its emission wavelength and enhancing its electron affinity. With this in mind, we identified the 9,10-dihydro-9,10-diboraanthracenes (DBAs, **I**; Scheme 1a) as a particularly promising molecular platform that can be modified in a variety of ways:[2] (i) π-extension of the core scaffold is straightforwardly possible through double electrophilic borylation of higher acenes,[3,4] and (ii) diverse halogenated derivatives are accessible,[5] allowing the introduction of various organyl substituents by Stille-type coupling reactions.[6]

However, an important structural motif that has not yet been realized is DBA derivatives carrying strongly Lewis-basic heteroatom substituents. One reason is that the most common

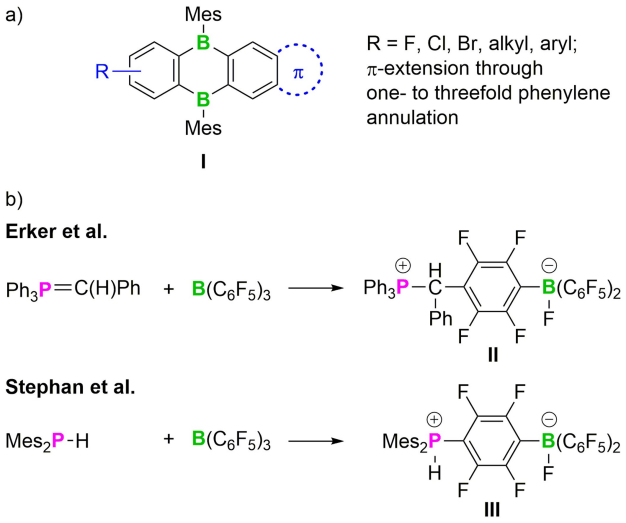

Scheme 1. a) General structure **I** of a mesityl-protected 9,10-dihydro-9,10-diboraanthracene (DBA) showing possible derivatization modes through C-substitution and/or π-extension. b) Two rare cases of S_NAr reactions on fluorinated arylboranes.

[a] *T. Jin, Dr. M. Bolte, Dr. H.-W. Lerner, Prof. Dr. M. Wagner*
Institut für Anorganische Chemie
Goethe-Universität Frankfurt
Max-von-Laue-Strasse 7, 60438 Frankfurt (Main) (Germany)
E-mail: Matthias.Wagner@chemie.uni-frankfurt.de
Homepage: https://www.uni-frankfurt.de/58708118/wagner
[b] *Dr. J.-M. Mewes*
Mulliken Center for Theoretical Chemistry, Institut für Physikalische und Theoretische Chemie
Universität Bonn
Beringstraße 4, 53115 Bonn (Germany)
E-mail: janmewes@janmewes.de
Homepage: https://www.janmewes.de

Supporting information for this article is available on the WWW under https://doi.org/10.1002/chem.202202234

This publication is part of a Special Collection on aromatic chemistry in collaboration with the "19th International Symposium on Novel Aromatic Compounds (ISNA-19)".

protocols for DBA synthesis are based on cyclocondensation reactions involving Lewis acidic boron species as starting materials, intermediates, or primary products, which are incompatible with the presence of pre-installed Lewis donors in the precursor molecules.[2,7] Late-stage derivatization reactions are a potential alternative. Unfortunately, conventional electrophilic aromatic substitution reactions are not a viable option for the electron-deficient DBA core; Br/Li-exchange reactions on C-brominated DBAs and subsequent coupling with heteroatom halides failed in our hands and have also not been reported by other groups. One remaining solution to the problem would be a *nucleophilic* aromatic substitution on fluorinated DBAs. Precedence for such a derivatization mode comes from Erker et al., who observed substitution of one *para*-F atom in $B(C_6F_5)_3$ upon treatment with the phosphorus ylide $Ph_3P{=}C(H)Ph$ to give zwitterionic **II** under thermodynamic control (Scheme 1b).[8a] Likewise, Stephan et al. obtained the phosphonium borate **III** upon *para*-substitution of $B(C_6F_5)_3$ with $Mes_2P{-}H$, but called this an 'unusual reaction' (Scheme 1b).[8b,9] Indeed, corresponding S_NAr protocols are still virtually unexplored for the targeted derivatization of B-doped polycyclic aromatic hydrocarbons (B-PAHs).

Herein we show that the DBA derivative **P** (a dihydrodiborapentacene) with vicinal Ph_2P groups is accessible in high yields through an S_NAr reaction between $Ph_2P{-}SiMe_3$[10] and the difluorinated precursor **F** (Scheme 2).[3] We selected the phosphanyl substituents and their specific mutual configuration for the following reasons: (i) Compound **P** represents a novel type of Frustrated Lewis Pair (FLP),[11] with potential B···B,[2] P···P, and B···P cooperativity. (ii) The π-donor substituent Ph_2P can be straightforwardly transformed into a strong σ/π-acceptor by oxidation or alkylation, which is a powerful tool for preparing DBAs with unprecedentedly low LUMO-energy levels.[13] (iii) The role of the chelating 1,2-bis(diphenylphosphanyl)benzene (dppb) ligand in the fields of homogeneous catalysis[14] and luminescent coordination complexes is well established.[15] Compound **P** should also act as an efficient transition-metal ligand - but this time with an electron-depleted backbone and possible applications in photocatalysis.[16] The π-extended core skeleton of **P** was preferred over a mere DBA framework, because of its superior photoluminescence properties,[3] which allow a better assessment of the influence of different P-substituents on this important parameter.

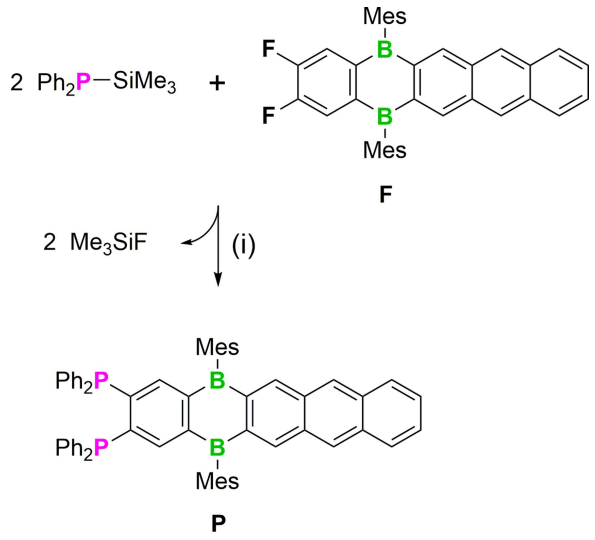

Scheme 2. Synthesis of the doubly Ph_2P-substituted dihydrodiborapentacene **P** by nucleophilic substitution of the two F atoms in **F** using a silylphosphane. (i) C_6H_6, 180 °C, 3 d, sealed thick-walled glass ampoule; quantitative conversion by NMR, 77% yield.[12]

Results and Discussion

Synthesis of P–[PAg]$_2$: The difluorinated starting material **F** (Scheme 2) was synthesized according to a literature procedure.[3] Initial attempts at introducing the phosphanyl substituents by treatment of **F** with $Ph_2P{-}H$ (C_6D_6, 100–160 °C, 2 d; sealed NMR tube) did not lead to an appreciable reaction. The use of $Ph_2P{-}Li$ (THF, rt) or $Ph_2P{-}SnMe_3$ (C_6D_6, 80–160 °C, 2 d; sealed NMR tube) resulted in significant decomposition of the DBA. However, heating **F** with a tenfold excess of $Ph_2P{-}SiMe_3$ gave a quantitative conversion to **P** (C_6H_6, 180 °C, 3 d; sealed thick-walled glass ampoule); after removal of the solvent at room temperature under reduced pressure, unconsumed $Ph_2P{-}SiMe_3$ can be recovered from the liquid residue by distillation (130 °C, 10^{-3} torr). **P** was finally purified by reprecipitation/recrystallization from an *n*-hexane-CH_2Cl_2 mixture (4:1; 77% yield).

In contrast to Ph_3P, which is relatively air stable and can be stored under ambient atmosphere for extended periods,[17] compound **P** undergoes quantitative aerial oxidation to the corresponding phosphine oxide **PO** under daylight within 10 h (Scheme 3). Importantly, no detectable oxidation occurs under otherwise similar conditions in the dark (NMR-spectroscopic control). We take this as an indication of a pronounced light-induced charge transfer (CT) from the Ph_2P substituents to the B-PAH π-electron system, opening possibilities for the use of **P** as a ligand for redox photocatalysts. We found in this context that **F** catalyzes the oxidation of Ph_3P by air under ambient light (CH_2Cl_2, 10 h; quantitative conversion to Ph_3PO according to NMR spectroscopy, no detectable degradation of **F**). No significant Ph_3P oxidation occurs in the same time interval, when either light is excluded from the solution or **F** is omitted. If **F** is replaced by anthracene as the photocatalyst, only 15% conversion of Ph_3P to Ph_3PO occurs (NMR-spectroscopic control).

For comparison with the phosphine oxide **PO**, we also prepared the phosphine sulfide **PS** from **P** and S_8 with quantitative conversion and in 83% yield (Scheme 3).

Methylation of the Ph_2P substituents in **P** would not only increase their formal oxidation states from P(III) to P(V), but also introduce two positive charges in close proximity to the B-PAH, which should further facilitate electron uptake. The corresponding product [**PMe**][BF_4]$_2$ was obtained in 63% yield by using an excess of the Meerwein salt [Me_3O][BF_4] (CH_2Cl_2, 100 °C, 6 h; sealed glass ampoule; Scheme 3).

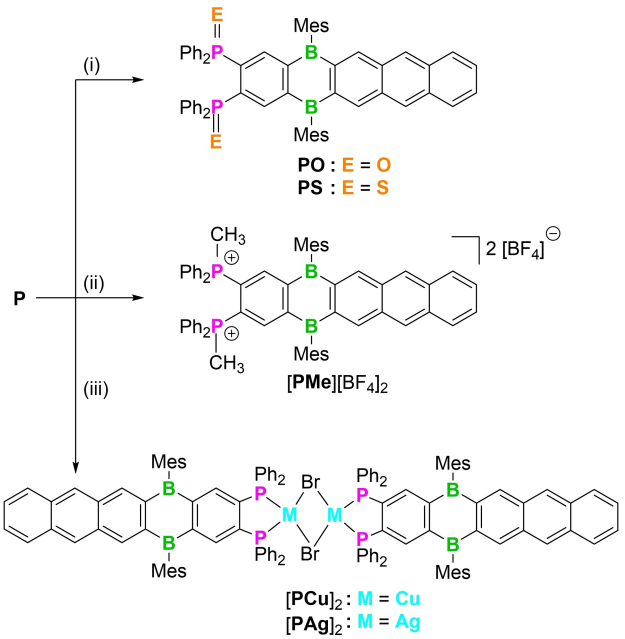

Scheme 3. Synthesis of **PO**, **PS**, and [**PMe**][BF_4]$_2$ with formal P(V) substituents. Complexation of **P** with CuBr and AgBr to afford [**PCu**]$_2$ and [**PAg**]$_2$, respectively. (i) **PO**: ambient air, CH_2Cl_2, rt, daylight, 10 h; quantitative conversion by NMR, 71% yield; **PS**: 1.5 equiv. S atoms, C_6H_6, 100 °C, 12 h; quantitative conversion by NMR, 83% yield. (ii) exc. [Me_3O][BF_4], CH_2Cl_2, 100 °C, 6 h, sealed thick-walled glass ampoule; 63% yield. (iii) [**PCu**]$_2$: 1.5 equiv. CuBr, CH_2Cl_2, rt, 12 h; 96% yield; [**PAg**]$_2$: 1.5 equiv. AgBr, CH_2Cl_2, rt, 12 h; 94% yield.[12]

Finally, we tested the chelating abilities of **P** toward positively charged Cu(I) and Ag(I) ions: Treatment of **P** with 1.5 equiv. of CuBr or AgBr (CH_2Cl_2, rt, 12 h) led to the formation of 1:1 complexes (>90% yield) that crystallized from *n*-hexane-CH_2Cl_2 mixtures as dimers [**PCu**]$_2$ or [**PAg**]$_2$ with central M–(μ-Br)$_2$–M units (M = Cu, Ag; Scheme 3).

NMR-spectroscopic and crystallographic characterization of P–[PAg]$_2$: All NMR spectra were recorded in CD_2Cl_2. The characteristic ^{31}P NMR shifts of the compounds obtained follow the same trend as those of representative model systems: δ(**P**) = −13.4 (Ph_3P: −5.5,[18] dppb: −13.2[19]), δ(**PO**) = 29.9 (Ph_3PO: 30.3[20]), δ(**PS**) = 46.7 (Ph_3PS: 44.6[20]), δ([**PMe**][BF_4]$_2$) = 25.6 ([Ph_3PMe][BF_4] = 21.5[21]), δ([**PCu**]$_2$) = −20.3 ({Cu(μ-Br)dppb}$_2$: −19.0[15a]), and δ([**PAg**]$_2$) = −5.3 ({Ag(μ-Br)dppb}$_2$: −4.3[15b]). As in the literature examples, the signals of the two complexes [**PCu**]$_2$ and [**PAg**]$_2$ are strongly broadened, one reason probably being the unresolved ^1J(P,M) coupling; in the case of [**PCu**]$_2$, quadrupolar broadening due to the coordinated Cu(I) ions is also likely to play a role (^{63,65}Cu: S = 3/2, 3/2; 69%, 31%).[22]

The ^{11}B NMR signals of **P**, **PO**, and **PS** are very broad and appear in the narrow range between 68–74 ppm, typical of tricoordinated boron nuclei;[22] the resonances of [**PMe**]$^{2+}$, [**PCu**]$_2$, and [**PAg**]$_2$ are broadened beyond detection.

The electron-donating or -withdrawing effects of the different P-substituents on the electronic structure of the B-PAH were assessed by ^{13}C{^{1}H} NMR spectroscopy.[23] The results are discussed in the Supporting Information (page S8).

The solid-state structures of **P**, **PS**, [**PCu**]$_2$ (Figure 1), and [**PAg**]$_2$ (Figure S48) were characterized by X-ray crystallography. In **P**, the orientation of the two Ph_2P groups relative to the dihydrodiborapentacene moiety is such that one Ph–P vector of each Ph_2P substituent is almost orthogonal to the attached C_6H_2 ring (torsion angles C(61)–P(1)–C(4)–C(5) = 82.8(4)°, C(81)–P(2)–C(5)–C(4) = 95.5(4)°). These two vectors point in opposite directions. The bond angles P(1)–C(4)–C(5) = 118.2(4)°, P(2)–C(5)–C(4) = 119.2(4)° are close to the ideal value of 120°, which argues against any notable steric repulsion between the two Ph_2P substituents (P···P distance: 3.187(2) Å). All in all, the structural parameters of the $(Ph_2P)_2C_6H_2$ fragment in **P** agree well with those of the free dppb ligand.[24]

The relative conformation of the two Ph_2P substituents in **PS** remains the same as in the case of **P**. However, the sum of C–P–C angles about P(1) and P(2) is increased from 304° in **P** to 315° in **PS** and the P···P distance is expanded to 3.613(2) Å. The P=S bonds amount to P(1)–S(1) = 1.943(2) Å and P(2)–S(2) = 1.951(2) Å and are thus comparable to the corresponding bonds in Ph_3PS (1.950(3) Å[25]).

The solid-state structures of [**PCu**]$_2$ and [**PAg**]$_2$ are very similar, so only the Cu(I) complex is discussed here. [**PCu**]$_2$ forms a C_1-symmetric, Br-bridged dimer with a folded four-membered Cu_2Br_2 core (Cu···Cu = 2.940(1) Å, Cu(1)Br_2//Cu(2)Br_2 = 42.0(1)°). The average Cu–P (2.275 Å) and Cu–Br (2.480 Å) bond lengths are close to those of the dimeric complex {Cu(μ-Br)dppb}$_2$.[15a]

Optoelectronic properties of P–[PAg]$_2$: Cyclic voltammograms were measured in CH_2Cl_2 ([nBu$_4$N][PF_6]; vs. FcH/FcH$^+$; Figure 2, Table S1). The free phosphine **P** undergoes reversible reduction at $E_{1/2}$ = −1.89 V. As anticipated, phosphorus oxidation has a pronounced effect on the redox potential of the dihydrodiborapentacene fragment, as **PO** is reducible already at

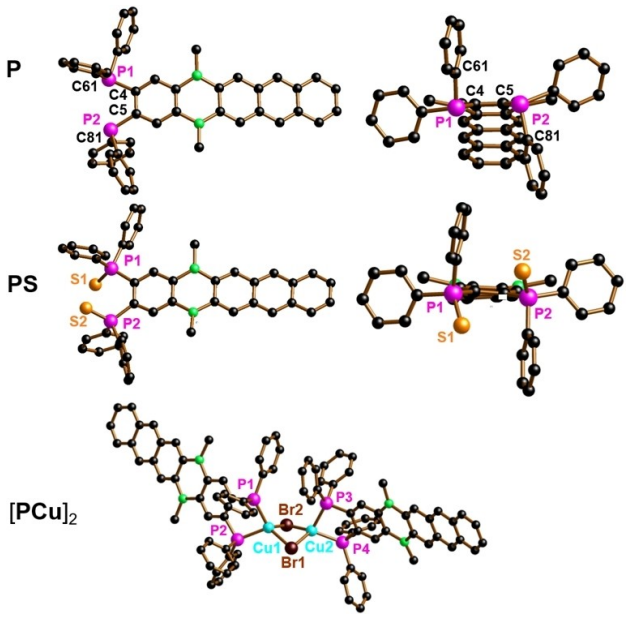

Figure 1. Crystallographically determined solid-state structures of **P**, **PS**, and [**PCu**]$_2$; H atoms and all mesityl-C atoms (except the *ipso* atoms C_i) have been omitted for clarity.

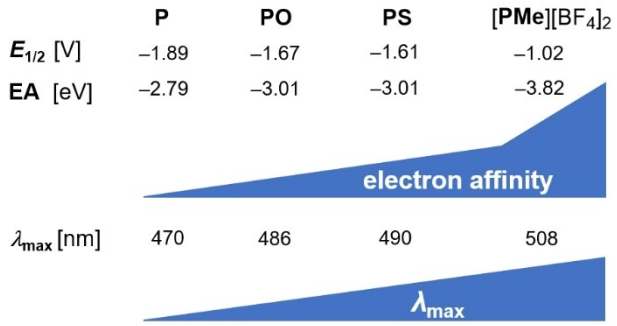

Figure 2. Top: $E_{1/2}$ values for the reduction (CH_2Cl_2, 0.1 M [nBu$_4$N][PF$_6$]; vs. FcH/FcH$^+$) and calculated electron affinities (EA) (ΔSCF/B3LYP-D4/def2-TZVP(-f)/SMD(CH_2Cl_2) using the relaxed structures) of compounds **P**, **PO**, **PS**, [**PMe**][BF$_4$]$_2$, and the resulting trend in their electron affinities; bottom: longest-wavelength absorption maxima λ_{max} of **P**, **PO**, **PS**, [**PMe**][BF$_4$]$_2$ (C_6H_6).

$E_{1/2} = -1.67$ V (**PO**–**P** = 0.22 eV) and **PS** at $E_{1/2} = -1.61$ V (**PS**–**P** = 0.28 eV). The most dramatic change toward a higher electron affinity occurs upon double methylation of the P substituents: the reduction potential of [**PMe**][BF$_4$]$_2$ of $E_{1/2} = -1.02$ V ([**PMe**][BF$_4$]$_2$–**P** = 0.87 eV) is anodically shifted - even relative to $E_{1/2} = -1.26$ V of octafluorinated DBA.[5] The electron affinity of [**PMe**][BF$_4$]$_2$ thus rivals that of the fullerene C_{60},[26] an indispensable electron acceptor in organic photovoltaics.[27]

The observed trends in the reduction potentials are in good agreement with theory (Figure 2). At the ΔSCF/B3LYP-D4/def2-TZVP(−f)/SMD(CH_2Cl_2) level of theory with full structural relaxation of the neutral species, anions, and cations,[28] the electron-affinity (EA) of **P** is calculated at −2.79 eV (Figure 3). For **PO** and **PS**, the EAs increase by absolute values of 0.22 eV (to −3.01 eV), which is in reasonable agreement with the experimental Δ values of 0.22 and 0.28 eV, respectively. Most importantly, the calculated EA = −3.82 eV of the dication [**PMe**]$^{2+}$ is 1.03 eV larger than that of **P**, which again agrees well with the observed behavior (experimental Δ = 0.87 eV).

The highest occupied and lowest unoccupied molecular orbitals (HOMO and LUMO) of **P**, **PO**, **PS**, and [**PMe**]$^{2+}$ are shown in Figure 3, together with the calculated orbital energies, ionization potentials (IPs) and EAs. The HOMOs of all four compounds are strictly localized on their 2,3-anthrylene fragments (in the following termed "An"); only in the case of **P**, there are contributions from the electron lone-pairs on the two P atoms and from the attached phenylene ring, as evident from the transparent surfaces. This mixing occurs because the molecular orbital dominated by these lone-pairs exists only in **P** and lies energetically just below the HOMO (HOMO-1 at −5.83 eV, 0.19 eV below the HOMO). The LUMOs show major contributions from the vacant B(p_z) orbitals and from directly adjacent C atoms, as well as from those C atoms carrying the $Ph_2P(E)$ substituents (solid surfaces), while minor contributions (transparent surfaces) are more distributed.

UV/vis absorption and emission spectra were recorded in CH_2Cl_2 and C_6H_6 (Tables S1, S2); in the following, we are discussing mainly data obtained on C_6H_6 solutions. The UV/vis absorption spectra of compounds **P** (yellow), **PO** (yellow-orange), and **PS** (orange) are qualitatively the same (as a representative example, the spectrum of **PO** in C_6H_6 is shown in Figure 4). All three spectra show longest-wavelength absorptions with resolved vibrational fine structures. The most bathochromically shifted maximum of **P** is observed at $\lambda_{max} = 470$ nm (2.64 eV), of **PO** at 486 nm (2.55 eV), and of **PS** at 490 nm (2.53 eV), indicating that an increasing electron-accept-

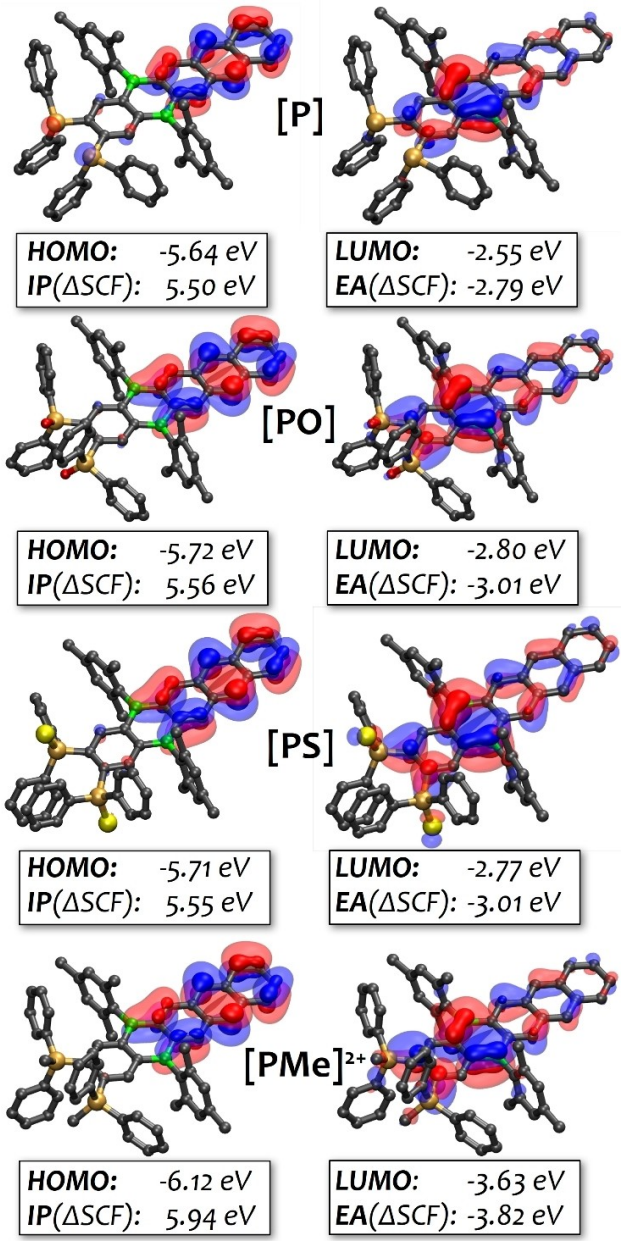

Figure 3. Plots of the highest occupied and lowest unoccupied molecular orbitals (HOMO and LUMO) of **P**, **PO**, **PS**, and the dication [**PMe**]$^{2+}$. The orbitals and corresponding energy levels were calculated at the B3LYP-D4/def2-TZVP(-f)/C-PCM(CH_2Cl_2) level of theory, while the ionization potentials (IP) and electron affinities (EA) are based on a more elaborate relaxed ΔSCF approach with the SMD solvation model (same functional and basis set; see discussion). Visualization with VMD 1.9.4 using an isovalue of 0.06 (meaning the enclosed volume contains 94% of the electron density of this orbital) for the solid surfaces (major contributions) and 0.02 (corresponding to 98% enclosed electron density) for the transparent surfaces (minor contributions).

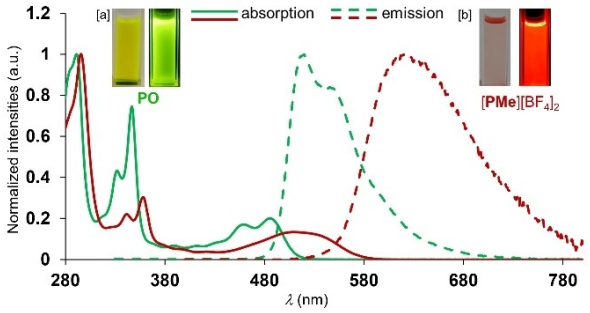

Figure 4. Normalized UV/vis absorption and emission spectra of **PO** (green lines) and [**PMe**][BF_4]$_2$ (red lines) in C_6H_6. [a] Solution of **PO** under ambient light (left) and UV light (366 nm, right). [b] Solution of [**PMe**][BF_4]$_2$ under ambient light (left) and UV light (366 nm, right). **PO**: λ_{ex} = 290 nm, [**PMe**][BF_4]$_2$: λ_{ex} = 295 nm.

or quality of the P substituents facilitates the associated electron transitions. Of **P**, **PO**, and **PS**, only **PO** is appreciably emissive and generates green luminescence with λ_{em} = 521 nm (2.38 eV, Φ_{PL} = 75 %, C_6H_6; Figure 4). A marked solvatochromism indicates some CT character of the electron transition (cf. λ_{em} = 521 nm (C_6H_6) vs. 539 nm (CH_2Cl_2)). A switch from **PO** to the dicationic [**PMe**]$^{2+}$ results in a pronounced further red shift of the longest-wavelength absorption maximum, which now appears at λ_{max} = 508 nm (2.44 eV) and has lost its vibrational fine structure (C_6H_6). A red emission is observed at λ_{em} = 622 nm (1.99 eV, Φ_{PL} = 19 %, C_6H_6; Figure 4).

To explore the character and properties of the low-lying excited states, we conducted time-dependent DFT (TDDFT) calculations[29] in the Tamm-Dancoff approximation (TDA)[30] with the optimally-tuned range-separated LRC-ωPBEh functional[31] and the pt(SS + LR)-PCM non-equilibrium solvation model (see the Supporting Information for computational details).[32,33] We specifically chose this combination of methods as it compensates for most of the shortcomings of TDDFT in describing CT states in dielectric environments.

This is necessary because, as already suspected, the lowest vertical excitations of all four molecules are dominated by two different types of CT: (1) There is a strongly allowed class of CT states (calculated oscillator strengths (f_{osc}) ≈0.2–0.5), in which charge is shifted from the outer regions of the large aromatic system toward the vacant B(p_z) orbitals ("in-plane CT"; note that the charge can originate either from the electron lone-pairs at the Ph_2P substituents ("P-to-B"; Figure 5a) or from the 2,3-anthrylene unit ("An-to-B"; Figure 5b)). (2) An optically forbidden class of CT states (calculated f_{osc} < 0.01) is characterized by transitions from the mesityl (Mes) substituents to the vacant B(p_z) orbitals ("Mes-CT"; Figure 5c). In some cases, if the energies of several different CT states are very close, mixtures between these states are also observed.

For **P**, the calculations reveal that the three lowest-energy excited states have more or less mixed CT character: As evident from the solid surfaces in Figure 5, the strongly allowed S_1 and S_2 states are dominated by "P-to-B" and "An-to-B" (in-plane) CT. S_3 is mainly a dark "Mes-CT" state. In stark contrast to **P**, the lowest excited state (S_1) of **PO** exhibits pure "Mes-CT" character

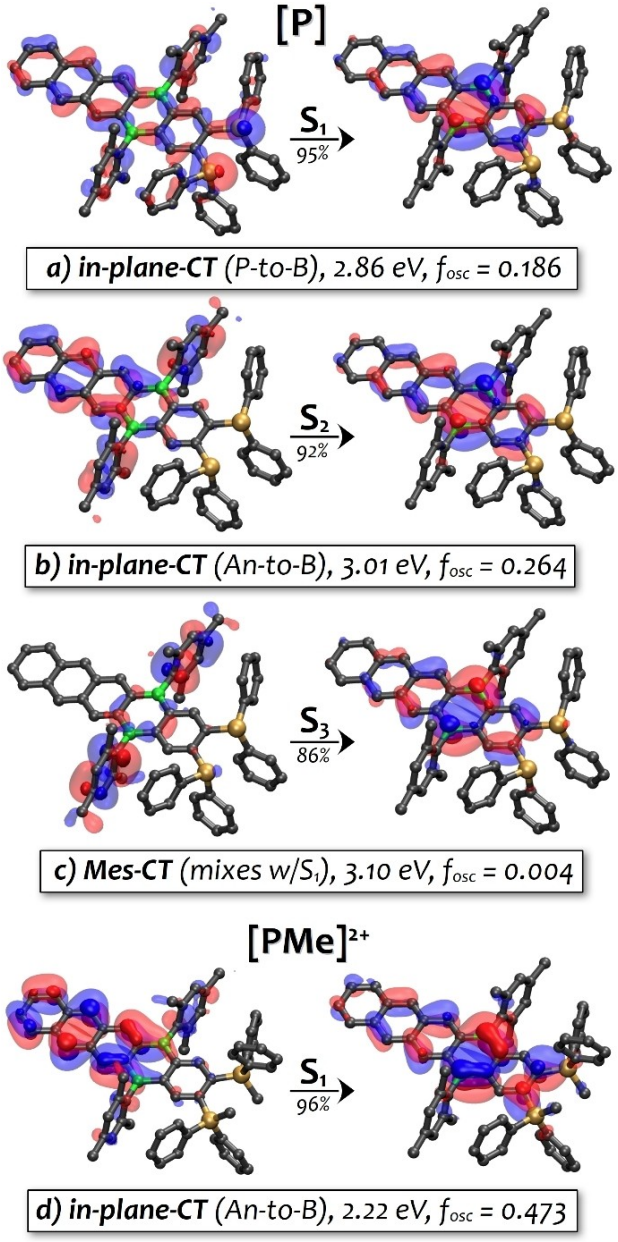

Figure 5. Visualization of the dominant natural transition orbital (NTO) pairs of a representative set of "in-plane CT" (a, b, d) and "Mes-CT" (c) states of **P** and the dication [**PMe**]$^{2+}$. The respective states of **PO** and **PS** are very similar (NTO pairs for the lowest excited states of all molecules can be found in the Supporting Information). The weights of the shown NTO pairs are given underneath the arrows. TDA-DFT calculations at the OT-LRC-ωPBEh/def2-TZVP level of theory with pt(SS + LR)-PCM solvation with parameters for toluene based on B3LYP-D4/def2-TZVP(-f)/C-PCM optimized structures. Calculations and visualizations were conducted with identical settings as in Figure 3.

and is dark (2.92 eV, f_{osc} = 0.006), while S_2 is a near-degenerate "An-to-B in-plane CT" and thus strongly allowed (2.92 eV, f_{osc} = 0.396). The situation for **PS** is similar to that of **PO**, with a dark "Mes-CT" (S_1; 2.86 eV, f_{osc} < 0.001) and a strongly allowed S_2 of "in-plane CT" character (2.89 eV, f_{osc} = 0.497), both attaining slightly lower energies than in the case of **PO**. Finally, for [**PMe**]$^{2+}$, TDDFT predicts distinctly lower excitation energies for

S1 ("in-plane CT", 2.22 eV, $f_{osc}=0.473$) and S_2 ("Mes-CT", 2.39 eV, $f_{osc}=0.007$). Hence, although the calculated excitation energies are somewhat too high for **P**, **PO**, and **PS**, and too low for [**PMe**]$^{2+}$, the general trends are well reproduced. We assume that the observed discrepancies are due to the neglect of vibronic couplings in the calculations, which strongly influence the absorption process, as evident from the vibrational fine structure in the recorded absorption spectra. The emissive properties of **P**–[**PMe**]$^{2+}$ were explored by excited-state optimizations of their "in-plane CT" and "Mes-CT" states (see the Supporting Information for more details). For **P**, due to severe state mixing, all excited-state optimizations eventually converge to the "P-to-B in-plane CT" state. The emission energy decreases during optimization from 2.90 eV to 1.03 eV. This is accompanied by the formation of a P···P interaction (see Figure S49), which provides an efficient radiationless decay channel and indicates why **P** is not fluorescent.

In contrast to **P**, only minor structural changes are observed during optimization of the "in-plane CT" states of **PO** and **PS**; the same applies to the optimization of their dark "Mes-CT" states. The calculated emission energies/f_{osc} for the "in-plane CT" remain relatively high at 2.56 eV (484 nm)/0.559 (**PO**) and 2.48 eV (500 nm)/0.640 (**PS**) and agree reasonably well with the experimental data for **PO** (2.38 eV, 521 nm). Computed emission energies and f_{osc} values for the "Mes-CT" are distinctly lower. Concerning the energetic ordering in the relaxed regime, the calculations predict the dark "Mes-CT" states to be near-degenerate with (**PO**) or slightly below (**PS**) the emitting "in plane-CT" states in both molecules. However, these respective energy differences ($\Delta=0.003$ eV (**PO**), 0.03 eV (**PS**) vs. $kT^{300K}=0.025$ eV) are not large enough to explain why **PO** is emissive while **PS** is not. For [**PMe**]$^{2+}$, all excited-state optimizations eventually converge to the "in-plane CT" state, which is the lowest excited state (by 0.1 eV) already at the ground-state structure. The large $f_{osc}=0.556$ and the emission energy of 1.99 eV (623 nm) agree with the experimentally observed strongly emissive behavior.

The UV/vis spectra of the Cu(I) and Ag(I) complexes [**PCu**]$_2$ and [**PAg**]$_2$ are very similar to that of **P** with pronounced long-wavelength absorptions at $\lambda_{max}=473$ and 489 nm. However, especially in the spectrum of [**PCu**]$_2$, an extremely broad feature of low intensity appears approximately between 530–640 nm (Figure 6). This additional band is assignable to additional low-lying states in the [**PCu**]$_2$ complex (S_1–S_4), the energetically lowest of which (S_1) is strongly allowed with $f_{osc}=0.221$ at 2.11 eV (589 nm). A similar state is also found in [**PAg**]$_2$, albeit at a higher energy of 2.44 eV (509 nm, $f_{osc}=0.372$). In general, these states are characterized by the transfer of an electron from mixed M(d)/P(p) orbitals (HOMO and HOMO−1 of the respective complex, localized at the [$P_2M(\mu\text{-Br})_2$ core; M = Cu, Ag), to the vacant B(p_z) orbitals (LUMO and LUMO+1 of the respective complex; Figure 7). Accordingly, compared to the ground state, the Mulliken charge of the [$P_2Cu(\mu\text{-Br})]_2$ core becomes more positive by 0.7 e^- in S_1 (based on the unrelaxed TDDFT density). The frontier orbitals of [**PCu**]$_2$, as well as the dominant natural transition orbital (NTO) pair for the lowest transition (S_1), are visualized in Figure 7; the dominant NTO pairs for S_2–S_4 are provided in the Supporting Information. Inspection of these NTO plots reveals that S_1–S_4 are different permutations of the same basic metal-to-ligand MLCT state (CT from each of the two metal centers to each of the B_2C_4 acceptor units). Owing to the much larger electron-hole separation in these MLCT states, they are significantly more polar than the respective "in-plane CT" and "Mes-CT" states of **P**, **PO**, and **PS**. This, in turn, leads to a stronger coupling to the environment and explains their much broader absorption feature. Note that these states are really an addition, while the 'original' CT states localized on the ligand **P** are also still present. The TDDFT calculations show that they are almost unchanged in [**PCu**]$_2$ (cf. S_9 at 2.94 eV ($f_{osc}=0.238$) and S_{11} at 2.97 eV ($f_{osc}=0.330$), corresponding to S_1 and S_2 of **P**, respectively), which explains the similarity of the two absorption spectra of **P** and [**PCu**]$_2$.

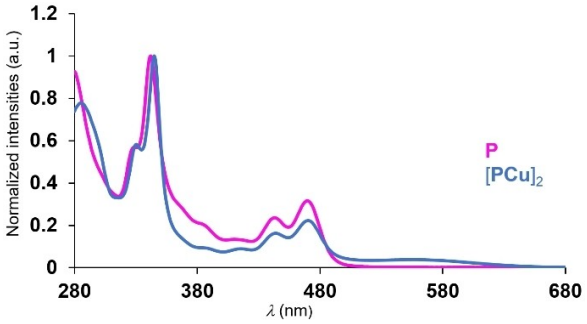

Figure 6. Normalized UV/vis absorption spectra of **P** (pink line) and [**PCu**]$_2$ (blue line) in C_6H_6.

Conclusion

We introduce the 5,14-dihydro-5,14-diborapentacene (DBP) **P**, endowed with two vicinal Ph_2P groups in its 2,3-positions. Ambipolar **P** thus combines strongly electron-donating and -accepting functionalities. The nucleophilic aromatic substitution protocol developed for the synthesis of **P** should have a broad scope and should also be useful for the preparation of other heteroatom-containing B-doped polycyclic aromatic hydrocarbons (B-PAHs). Upon light irradiation, **P** undergoes P-to-B CT, as confirmed by UV/vis absorption spectroscopy and quantum-chemical calculations. This finding is relevant in the context of recent reports on the formation of $[R_3P^{\bullet}]^+[R'_3B^{\bullet}]^-$ frustrated radical pairs (FRPs) within B/P FLPs and corresponding claims that radicals may play an important role in FLP chemistry.[34] The FRPs reported so far are formed by *inter*molecular CT within the encounter complex, whereas in the case of **P**, the photoinduced CT is an *intra*molecular process. Correspondingly, photoexcitation by ambient light in air results in remarkably facile oxidation of both Ph_2P groups to furnish $Ph_2P(O)$ moieties. In turn, the electron affinity of the resulting compound **PO** increases by an absolute value of 0.22 eV; an even larger increase is achievable by double P methylation ($|\Delta|=0.87$ eV). The two Ph_2P substituents in **P** consequently provide an excellent tool for targeted modulation of the DBP-LUMO

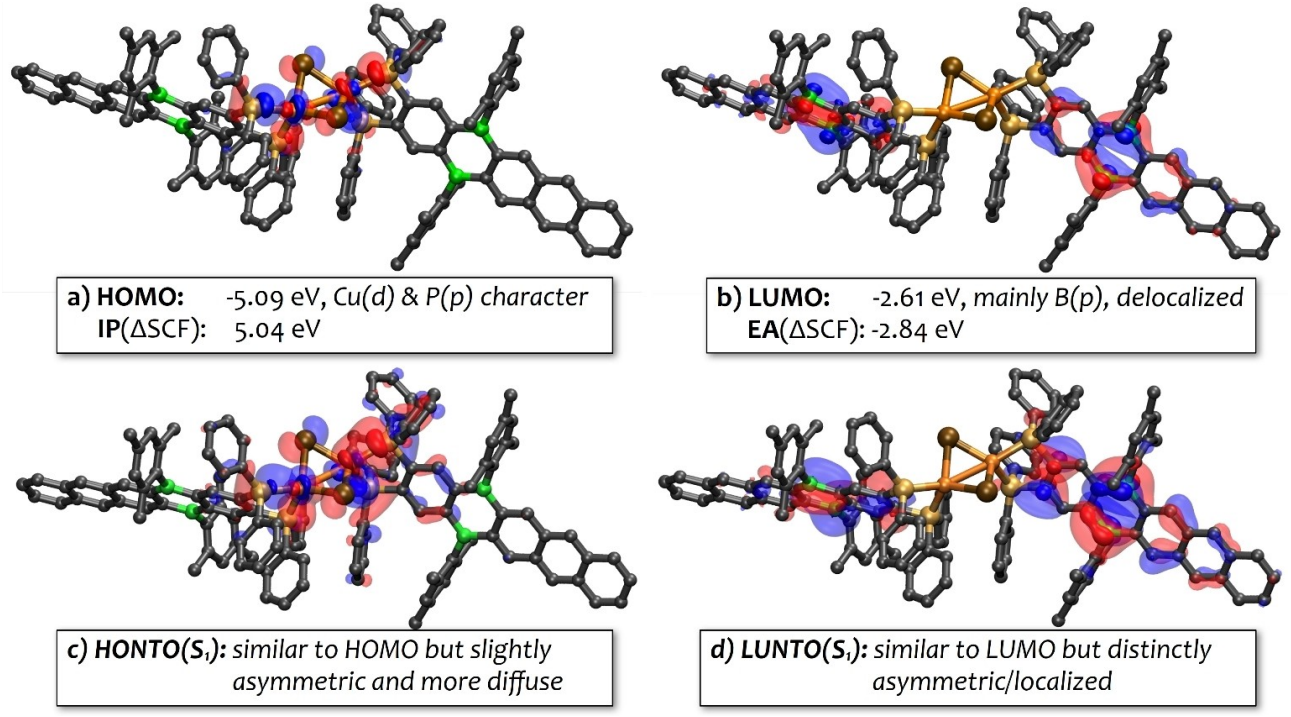

Figure 7. Plots of the highest occupied and lowest unoccupied molecular orbital (HOMO and LUMO) of [**PCu**]$_2$, together with the dominating natural transition orbital pair (HONTO and LUNTO) of its lowest excited singlet state, S_1. The corresponding HONTO and LUNTO pairs for S_2–S_4 are very similar (permutations of the two **P** moieties and metal centers of the complex) and are provided in the Supporting Information. Calculations and visualizations were conducted with identical settings as in Figures 3 and 5.

level (Figure 2). Alternatively, they can be used to chelate coinage-metal salts, such as CuBr and AgBr, to afford dimeric complexes [**PCu**]$_2$ and [**PAg**]$_2$ with [M(μ-Br)]$_2$ cores ($M^+ = Cu^+$, Ag^+).[35] The photophysics of these complexes is characterized by pronounced metal-to-ligand charge transfer (MLCT), as confirmed by state-of-the-art quantum-chemical calculations. We are presently exploring possibilities of using transition-metal complexes of **P**-type ligands as photocatalysts.

X-ray Crystallography

Deposition Numbers 2171458 (for **P**), 2171459 (for **PS**), 2171460 (for [**PCu**]$_2$), and 2171461 (for [**PAg**]$_2$) contain the supplementary crystallographic data for this paper. These data are provided free of charge by the joint Cambridge Crystallographic Data Centre and Fachinformationszentrum Karlsruhe Access Structures service.

Acknowledgements

T.J. is grateful to the China Scholarship Council for providing a Ph.D. scholarship. Open Access funding enabled and organized by Projekt DEAL.

Conflict of Interest

The authors declare no conflict of interest.

Data Availability Statement

The data that support the findings of this study are available in the supplementary material of this article.

Keywords: arylphosphines · charge transfer · diborapentacene · nucleophilic substitution · transition-metal complexation

[1] a) M. Stępień, E. Gońka, M. Żyła, N. Sprutta, *Chem. Rev.* **2017**, *117*, 3479–3716; b) L. Ji, S. Griesbeck, T. B. Marder, *Chem. Sci.* **2017**, *8*, 846–863; c) M. Hirai, N. Tanaka, M. Sakai, S. Yamaguchi, *Chem. Rev.* **2019**, *119*, 8291–8331; d) S. A. Iqbal, J. Pahl, K. Yuan, M. J. Ingleson, *Chem. Soc. Rev.* **2020**, *49*, 4564–4591.
[2] a) E. von Grotthuss, A. John, T. Kaese, M. Wagner, *Asian J. Org. Chem.* **2018**, *7*, 37–53; b) S. E. Prey, M. Wagner, *Adv. Synth. Catal.* **2021**, *363*, 2290–2309.
[3] a) A. John, M. Bolte, H.-W. Lerner, M. Wagner, *Angew. Chem. Int. Ed.* **2017**, *56*, 5588–5592; *Angew. Chem.* **2017**, *129*, 5680–5684; b) A. John, M. Bolte, H.-W. Lerner, G. Meng, S. Wang, T. Peng, M. Wagner, *J. Mater. Chem. C* **2018**, *6*, 10881–10887.
[4] For other ways of expanding the DBA core, see: a) S. Kirschner, J.-M. Mewes, M. Bolte, H.-W. Lerner, A. Dreuw, M. Wagner, *Chem. Eur. J.* **2017**, *23*, 5104–5116; b) A. John, S. Kirschner, M. K. Fengel, M. Bolte, H.-W. Lerner, M. Wagner, *Dalton Trans.* **2019**, *48*, 1871–1877; c) S. Kirschner, S. S. Bao, M. K. Fengel, M. Bolte, H.-W. Lerner, M. Wagner, *Org. Biomol. Chem.* **2019**, *17*, 5060–5065.

[5] a) C. Reus, N. W. Liu, M. Bolte, H.-W. Lerner, M. Wagner, *J. Org. Chem.* **2012**, *77*, 3518–3523; b) S. Brend'amour, J. Gilmer, M. Bolte, H.-W. Lerner, M. Wagner, *Chem. Eur. J.* **2018**, *24*, 16910–16918.
[6] C. Reus, S. Weidlich, M. Bolte, H.-W. Lerner, M. Wagner, *J. Am. Chem. Soc.* **2013**, *135*, 12892–12907.
[7] a) E. Januszewski, A. Lorbach, R. Grewal, M. Bolte, J. W. Bats, H.-W. Lerner, M. Wagner, *Chem. Eur. J.* **2011**, *17*, 12696–12705; b) S. Luliński, J. Smétek, K. Durka, J. Serwatowski, *Eur. J. Org. Chem.* **2013**, 8315–8322.
[8] a) S. Döring, G. Erker, R. Fröhlich, O. Meyer, K. Bergander, *Organometallics* **1998**, *17*, 2183–2187; b) G. C. Welch, R. R. S. Juan, J. D. Masuda, D. W. Stephan, *Science* **2006**, *314*, 1124–1126.
[9] For very recent further examples, see: a) T. Jin, L. Kunze, S. Breimaier, M. Bolte, H.-W. Lerner, F. Jäkle, R. F. Winter, M. Braun, J.-M. Mewes, M. Wagner, *J. Am. Chem. Soc.* **2022**, *144*, 13704–13716; b) T. Jin, M. Bolte, H.-W. Lerner, M. Wagner, *Org. Chem. Front.* **2022**, DOI: 10.1039/d2qo01199a.
[10] D. W. Larsen, M. J. Boylan, S. E. Tunney, J. K. Stille, *J. Org. Chem.* **1987**, *52*, 748–753.
[11] a) G. Erker, D. W. Stephan, *Frustrated Lewis Pairs I & II*, Springer-Verlag Berlin, Heidelberg, 2013; b) D. W. Stephan, G. Erker, *Angew. Chem. Int. Ed.* **2010**, *49*, 46–76; *Angew. Chem.* **2010**, *122*, 50–81.
[12] For NMR monitoring, small-scale reactions were performed in the corresponding deuterated solvents.
[13] a) T. Baumgartner, R. Réau, *Chem. Rev.* **2006**, *106*, 4681–4727; b) C. R. Bridges, A. M. Borys, V. A. Béland, J. R. Gaffen, T. Baumgartner, *Chem. Sci.* **2020**, *11*, 10483–10487; c) C. Wang, M. Taki, Y. Sato, A. Fukazawa, T. Higashiyama, S. Yamaguchi, *J. Am. Chem. Soc.* **2017**, *139*, 10374–10381; d) J. D. R. Ascherl, C. Neiß, A. Vogel, J. Graf, F. Rominger, T. Oeser, F. Hampel, A. Görling, M. Kivala, *Chem. Eur. J.* **2020**, *26*, 13157–13162; e) Y. Sugihara, N. Inai, M. Taki, T. Baumgartner, R. Kawakami, T. Saitou, T. Imamura, T. Yanai, S. Yamaguchi, *Chem. Sci.* **2021**, *12*, 6333–6341.
[14] a) B. H. Lipshutz, Ž. v. Bošković, D. H. Aue, *Angew. Chem. Int. Ed.* **2008**, *47*, 10183–10186; *Angew. Chem.* **2008**, *120*, 10337–10340; b) T. Hatakeyama, Y. Kondo, Y. I. Fujiwara, H. Takaya, S. Ito, E. Nakamura, M. Nakamura, *Chem. Commun.* **2009**, 1216–1218; c) H. Chea, H. S. Sim, J. Yun, *Adv. Synth. Catal.* **2009**, *351*, 855–858; d) K. Motokura, N. Takahashi, D. Kashiwame, S. Yamaguchi, A. Miyaji, T. Baba, *Catal. Sci. Technol.* **2013**, *3*, 2392–2396.
[15] a) A. Tsuboyama, K. Kuge, M. Furugori, S. Okada, M. Hoshino, K. Ueno, *Inorg. Chem.* **2007**, *46*, 1992–2001; b) M. Osawa, I. Kawata, R. Ishii, S. Igawa, M. Hashimoto, M. Hoshino, *J. Mater. Chem. C* **2013**, *1*, 4375–4383.
[16] a) J. M. R. Narayanam, C. R. J. Stephenson, *Chem. Soc. Rev.* **2011**, *40*, 102–113; b) L. Marzo, S. K. Pagire, O. Reiser, B. König, *Angew. Chem. Int. Ed.* **2018**, *57*, 10034–10072; *Angew. Chem.* **2018**, *130*, 10188–10228.
[17] I. Ondrejkovičová, V. Vančová, G. Ondrejovič, *Chem. Pap.* **1991**, *45*, 35–40.
[18] M. Sun, H. Y. Zhang, Q. Han, K. Yang, S. D. Yang, *Chem. Eur. J.* **2011**, *17*, 9566–9570.
[19] S. E. Tunney, J. K. Stille, *J. Org. Chem.* **1987**, *52*, 748–753.
[20] T. Gáti, A. Simon, G. Tóth, D. Magiera, S. Moeller, H. Duddeck, *Magn. Reson. Chem.* **2004**, *42*, 600–604.
[21] C. Xu, T. Li, P. Jiang, Y. Zhang, *Tetrahedron* **2020**, *76*, 131107.
[22] J. Mason (ed.), *Multinuclear NMR*, Plenum Press, New York, 1987.
[23] a) N. S. Mills, E. E. Burns, J. Hodges, J. Gibbs, E. Esparza, J. L. Malandra, J. Koch, *J. Org. Chem.* **1998**, *63*, 3017–3022; b) R. Shenhar, R. Beust, S. Hagen, H. E. Bronstein, I. Willner, L. T. Scott, M. Rabinovitz, *J. Chem. Soc. Perkin Trans. 2.* **2002**, 449–454; c) C. Hoffend, M. Diefenbach, E. Januszewski, M. Bolte, H.-W. Lerner, M. C. Holthausen, M. Wagner, *Dalton Trans.* **2013**, *42*, 13826–13837; d) J. Gilmer, H. Budy, T. Kaese, M. Bolte, H.-W. Lerner, M. Wagner *Angew. Chem. Int. Ed.* **2020**, *59*, 5621–5625; *Angew. Chem.* **2020**, *132*, 5670–5674; e) H. Budy, T. Kaese, M. Bolte, H.-W. Lerner, M. Wagner, *Angew. Chem. Int. Ed.* **2021**, *60*, 19397–19405; *Angew. Chem.* **2021**, *133*, 19546–19554.
[24] W. Levason, G. Reid, M. Webster, *Acta Crystallogr.* **2006**, *C62*, o438–o440.
[25] P. W. Codding, K. A. Kerr, *Acta Crystallogr.* **1978**, *B34*, 3785–3787.
[26] C. A. Reed, R. D. Bolskar, *Chem. Rev.* **2000**, *100*, 1075–1120.
[27] a) N. S. Sariciftci, L. Smilowitz, A. J. Heeger, F. Wudl, *Science* **1992**, *258*, 1474–1476; b) Y. He, Y. Li, *Phys. Chem. Chem. Phys.* **2011**, *13*, 1970–1983.
[28] a) A. D. Becke, *J. Chem. Phys.* **1998**, *98*, 5648–5652; b) P. J. Stephens, F. J. Devlin, C. F. Chabalowski, M. J. Frisch, *J. Phys. Chem.* **1994**, *98*, 11623–11627; c) E. Caldeweyher, S. Ehlert, A. Hansen, H. Neugebauer, S. Spicher, C. Bannwarth, S. Grimme, *J. Chem. Phys.* **2019**, *150*, 154122; d) E. Caldeweyher, J.-M. Mewes, S. Ehlert, S. Grimme, *Phys. Chem. Chem. Phys.* **2020**, *22*, 8499–8512; e) A. V. Marenich, C. J. Cramer, D. G. Truhlar, *J. Phys. Chem. B* **2009**, *113*, 6378–6396.
[29] E. Runge, E. K. U. Gross, *Phys. Rev. Lett.* **1984**, *52*, 997–1000.
[30] S. Hirata, M. Head-Gordon, *Chem. Phys. Lett.* **1999**, *314*, 291–299.
[31] a) R. Baer, E. Livshits, U. Salzner, *Annu. Rev. Phys. Chem.* **2010**, *61*, 85–109; b) M. A. Rohrdanz, K. M. Martins, J. M. Herbert, *J. Chem. Phys.* **2009**, *130*, 054112.
[32] a) J.-M. Mewes, J. M. Herbert, A. Dreuw, *Phys. Chem. Chem. Phys.* **2017**, *19*, 1644–1654; b) J.-M. Mewes, Z. Q. You, M. Wormit, T. Kriesche, J. M. Herbert, A. Dreuw, *J. Phys. Chem. A* **2015**, *119*, 5446–5464.
[33] We computed the optoelectronic properties for the lowest-energy solution conformers of each compound, optimized at the B3LYP–D4 level and identified by the CREST conformer-search algorithm with the GFN2-xTB Hamiltonian in CH_2Cl_2 solution. Due to packing effects, the preferred orientations of the Ph_2P substituents of the same compound may differ in solution and in the solid state (see the Supporting Information for a detailed discussion).
[34] a) L. L. Liu, L. L. Cao, Y. Shao, G. Ménard, D. W. Stephan, *Chem.* **2017**, *3*, 259–267; b) Y. Soltani, A. Dasgupta, T. A. Gazis, D. M. C. Ould, E. Richards, B. Slater, K. Stefkova, V. Y. Vladimirov, L. C. Wilkins, D. Willcox, R. L. Melen, *Cell Rep. Phys. Sci.* **2020**, *1*, 100016; c) F. Holtrop, A. R. Jupp, B. J. Kooij, N. P. van Leest, B. de Bruin, J. C. Slootweg, *Angew. Chem. Int. Ed.* **2020**, *59*, 22210–22216; *Angew. Chem.* **2020**, *132*, 22394–22400; d) M. S. Hill, *Chem.* **2020**, *6*, 544–551.
[35] Compare works by Harman, who prepared DBAs (cf. **I**; Figure 1) carrying B-bonded *o*-phosphanylphenyl substituents (instead of Mes) and used them as Z-type ligands for the coordination of coinage-metal ions: a) J. W. Taylor, A. McSkimming, M. E. Moret, W. H. Harman, *Angew. Chem. Int. Ed.* **2017**, *56*, 10413–10417; *Angew. Chem.* **2017**, *129*, 10549–10553; b) J. W. Taylor, A. McSkimming, L. A. Essex, W. H. Harman, *Chem. Sci.* **2019**, *10*, 9084–9090; c) J. W. Taylor, W. H. Harman, *Chem. Commun.* **2020**, *56*, 4480–4483.

Manuscript received: July 17, 2022
Version of record online: September 12, 2022